AIAA 81-4021

Primitive-Variable Model Applications to Solid-Fuel Ramjet Combustion

Charles A. Stevenson* and David W. Netzer†
Naval Postgraduate School, Monterey, Calif.

An adaptation of a primitive-variable finite-difference computer program was accomplished in order to predict the reacting flowfield in a solid-fuel ramjet. The study compares the predictions of the primitive-variable computer model with predictions of an earlier stream function-vorticity computer model and with empirical data. The new model was found to be more readily adaptable to different geometric configurations and flow conditions. Flowfield calculations were made both within the fuel grain and the aft mixing chamber. Addition of the aft mixing chamber decreased the effect of fuel grain inlet velocity on boundery-layer thickness and the radial location of the flame zone within the fuel grain.

Nomenclature

A_{in} = area of air inlet
A_3 = area of fuel port
BP = mass transfer (or "blowing") parameter
C_1, C_2, C_D = K-ϵ model empirical constants (Table 1)
C_f = coefficient of friction
C_p = specific heat at constant pressure
E = 9.0
g = mass transfer conductance
G = air mass flux
h = enthalpy
$\tilde{h}$ = stagnation enthalpy
H = dimensionless enthalpy
i = stoichiometric coefficient
I = turbulence intensity
k = turbulence kinetic energy
m = mass fraction
$\dot{m}''$ = mass flux
p = pressure
$\dot{q}''$ = heat flux
r = radial distance
$\dot{r}$ = regression rate
S_ϕ = source term for variable ϕ
St = Stanton number
T = temperature
u = axial velocity
v = radial velocity
x = axial distance
y_p^+ = dimensionless distance from solid boundary
Γ = effective transport coefficient
δ = incremental distance from wall
ΔH = heat of combustion per kg of fuel
ϵ = turbulence dissipation rate
κ = von Kármán constant
μ = viscosity
ρ = density
σ = Prandtl or Schmidt number
τ = shear stress
ϕ = any dependent variable
χ = $m_{fu} - m_{ox}/i$

Subscripts

bw = fuel surface (or "blowing wall")
c = conserved
eff = effective
fg = fuel grain
fu = fuel
in = combustor inlet
lam = laminar
N2 = nitrogen
ox = oxygen
p = near-wall node
ref = reference
t = turbulent
w = wall

Received April 21, 1980; revision received Aug. 11, 1980. This paper is declared a work of the U.S. Government and therefore is in the public domain.

*Lieutenant, U.S. Navy.
†Associate Professor, Department of Aeronautics. Member AIAA.

Introduction

THE solid-fuel ramjet (SFRJ) is currently being considered as the propulsion device for a number of tactical applications. Examples are intermediate range air-to-air missiles and gun-launched projectiles. As the use of this propulsion device receives increased attention, it becomes more important that combustion models be developed which can be used to help determine optimum configurations and the most appropriate fuel composition.

A finite-difference solution of the governing fluid dynamic equations in terms of vorticity and stream function was applied to the SFRJ combustor in earlier publications.[1,2] That model provided reasonable agreement with experimental data taken within the fuel grain. Several problems were inherent to the model: 1) predicted pressure distributions were normally inaccurate, and 2) boundary conditions were difficult to specify. These characteristics limited the utility of the model. In a conventional application (Fig. 1), an aft mixing region is employed to allow for more complete combustion before the gases exit through the nozzle. It is important to be able to determine the combustion behavior within this region as a function of its geometry and of upstream conditions. It was very difficult to obtain converged solutions with the ψ-ω model when the aft mixing region was included after the fule grain.

Primitive-variable (velocity-pressure) models have shown promise for increased calculation accuracy, reduced computational time, and increased ease for the specification of boundary conditions in more complex geometries. One such model (CHAMPION 2/E/FIX) has been developed by Pun and Spalding.[3] Other investigators have used the same or similar methods for reacting turbulent flows.[4]

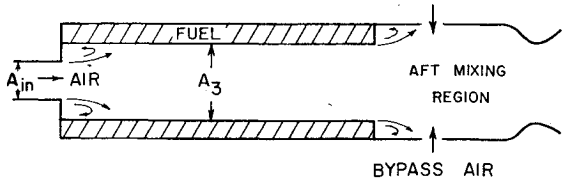

Fig. 1 Schematic of solid fuel ramjet.

The purpose of this investigation was to improve the modeling capabilities for the SFRJ by adapting the CHAMPION program to the SFRJ geometry and operating environment.

Model Overview

The flow was assumed to be steady, two-dimensional, and subsonic. For simplicity, the value of specific heat (C_p) was assumed to be constant although its dependence on temperature and/or composition could easily be included.

A modified Jones-Launder,[5-7] two-parameter turbulence model was incorporated to calculate the effective viscosity. It uses five empirical constants (Table 1) and requires that two additional variables [turbulence kinetic energy (k) and turbulence dissipation rate (ϵ)] be evaluated. Effective viscosity was calculated using the formulas

$$\mu_{\text{eff}} = \mu_{\text{lam}} + \mu_t \tag{1}$$

where

$$\mu_t = C_D \rho k^2 / \epsilon \tag{2}$$

For reacting flows, four species were considered: oxygen, nitrogen, fuel, and products. Simple, one-step, infinitely fast kinetics were assumed in which 1 kg of fuel combines with i kg of oxidant to form $(1+i)$ kg of product without intermediaries.[1,8] Fuel and oxygen, therefore, could not exist simultaneously, and the combustion process was mixing limited. In addition, it was assumed that no oxygen existed at the fuel surface and that that surface was isothermal. The turbulent Prandtl and Schmidt numbers were taken equal to unity, and therefore, the turbulent Lewis number was unity; the laminar Prandtl number was also taken to be unity.

The conservation equations for axisymmetrical flows with no tangential variations can be put into the general form[3]

$$\frac{\partial}{\partial x}(\rho u \phi) + \frac{1}{r}\frac{\partial}{\partial r}(\rho r v \phi) - \frac{\partial}{\partial x}\left(\Gamma_\phi \frac{\partial \phi}{\partial x}\right) - \frac{1}{r}\frac{\partial}{\partial r}\left(r\Gamma_\phi \frac{\partial \phi}{\partial r}\right) = S_\phi$$

convection terms diffusion terms source terms (3)

where ϕ stands for the dependent variables (u,v,k,ϵ,h, etc....) being considered ($\phi = 1$ for the continuity equation), Γ_ϕ is the appropriate effective exchange coefficient for turbulent flow, and S_ϕ is the "source term" (Table 2). The energy equation in terms of stagnation enthalpy has no source terms since the turbulent Prandtl and Schmidt numbers were chosen as unity and radiative transport was neglected. Thus, the stagnation enthalpy is given by

$$h = h + (u^2 + v^2)/2 + k \tag{4}$$

where for nonreacting flows

$$h \equiv C_p T \tag{5}$$

and for reacting flows

$$h \equiv m_{\text{ox}} \Delta H / i + C_p (T - T_{\text{ref}}) \tag{6}$$

Table 1 K-ϵ turbulence model empirical constants

C_1	C_2	C_D	$\sigma_{k,\text{eff}}$	$\sigma_{\epsilon,\text{eff}}$
1.43	1.92	0.09	1.0	1.3

Table 2 Governing equation parameters

ϕ	Γ_ϕ	S_ϕ
u	μ_{eff}	$-\frac{\partial p}{\partial x} - \frac{2}{3}\frac{\partial}{\partial x}\left\{\frac{\mu}{r}\left[\frac{\partial}{\partial x}(ru) + \frac{\partial}{\partial r}(rv)\right]\right\} + \frac{\partial}{\partial x}\left(\mu\frac{\partial u}{\partial x}\right) + \frac{1}{r}\frac{\partial}{\partial r}\left(\mu r \frac{\partial v}{\partial x}\right)$
v	μ_{eff}	$-\frac{\partial p}{\partial r} - 2\frac{\mu v}{r^2} - \frac{2}{3}\frac{\partial}{\partial r}\left\{\frac{\mu}{r}\left[\frac{\partial}{\partial x}(ru) + \frac{\partial}{\partial r}(rv)\right]\right\} + \frac{\partial}{\partial x}\left(\mu\frac{\partial u}{\partial r}\right) + \frac{1}{r}\frac{\partial}{\partial r}\left(\mu r \frac{\partial v}{\partial r}\right)$
k	$\frac{\mu_{\text{eff}}}{\sigma_k}$	$\mu_t\left\{2\left[\left(\frac{\partial u}{\partial x}\right)^2 + \left(\frac{\partial v}{\partial r}\right)^2 + \left(\frac{v}{r}\right)^2\right] + \left(\frac{\partial u}{\partial r} + \frac{\partial v}{\partial x}\right)^2\right\} - \rho\epsilon$
e	$\frac{\mu_{\text{eff}}}{\sigma_\epsilon}$	$\frac{C_1\epsilon}{k}\left\{\mu_t\left(2\left[\left(\frac{\partial u}{\partial x}\right)^2 + \left(\frac{\partial v}{\partial r}\right)^2 + \left(\frac{v}{r}\right)^2\right] + \left(\frac{\partial u}{\partial r} + \frac{\partial v}{\partial x}\right)^2\right)\right\} - \frac{C_2\rho\epsilon^2}{k}$
$\tilde{h}$	$\frac{\mu_{\text{eff}}}{\sigma_h}$	0
χ	$\frac{\mu_{\text{eff}}}{\sigma_j}$	0
m_{N2}	$\frac{\mu_{\text{eff}}}{\sigma_j}$	0

$\sigma_j = \sigma_k = \sigma_h = 1, \sigma_\epsilon = 1.3$

The calculation of temperature was made using Eqs. (4-6); density was calculated from the perfect gas law.

For modeling reacting flows, two additional quantities m_{N2} and $\chi \equiv m_{\text{fu}} - m_{\text{ox}}/i$ were evaluated. Each of these properties as well as stagnation enthalpy have identical governing differential equations [Eq. (3) with no source terms]. In appropriate dimensionless form, they also have identical boundary conditions. Thus, only one of the equations had to be solved. The dimensionless form selected for each property was

$$H = (\tilde{h}_{\text{in}} - \tilde{h})/(\tilde{h}_{\text{in}} - \tilde{h}_{fg}) \tag{7}$$

$$m_{\text{N2}} = (m_{\text{N2}_{\text{in}}} - m_{\text{N2}})/(m_{\text{N2}_{\text{in}}} - m_{\text{N2}_{fg}}) \tag{8}$$

$$\bar{\chi} = (\chi - \chi_{\text{in}})/(\chi_{fg} - \chi_{\text{in}}) \tag{9}$$

$$m_{\text{fu}} = \chi \quad m_{\text{ox}} = 0 \quad \text{for} \quad \chi \geq 0$$

$$m_{\text{fu}} = 0 \quad m_{\text{ox}} = -\chi i \quad \text{for} \quad \chi < 0 \tag{10}$$

Boundary Conditions and Solution Procedure

Fixed boundary conditions (inlet velocity profile, etc....) were specified at the desired or experimentally determined

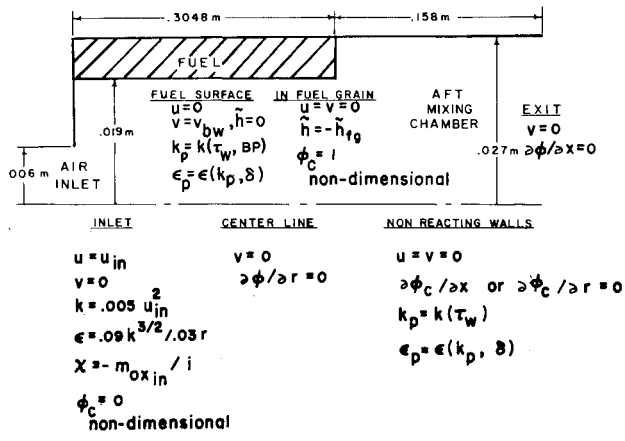

Fig. 2 SFRJ geometry and boundary conditions.

values. Specified gradient boundary conditions were handled by setting the appropriate convection/diffusion coefficient to zero in the finite-difference equation ("breaking the link") and then entering the appropriate gradient through linearized "false" source terms.[3] The geometry and appropriate boundary conditions are summarized in Fig. 2.

Although not a computer program limitation, "plug flow" was assumed at the inlet. Turbulence kinetic energy was selected to be uniform with a value which corresponded to the approximate turbulence intensity of the inlet flow. Radial and axial gradients were set equal to zero on the centerline and exit, respectively. In addition, all nonreacting solid boundaries were considered adiabatic with both velocity components equal to zero ("no slip" condition).

For simplicity, a two-part boundary layer was used. The border between the laminar sublayer and the turbulent layer was taken at[3] $y_p^+=11.5$. y_p^+ was evaluated at each near-wall node (p)

$$y_p^+=(\rho\delta/\mu_{\text{lam}})(\tau_w/\rho)^{1/2} \tag{11}$$

where for $y_p^+\geq 11.5$,

$$\tau_w=C_D^{1/2}\rho k_p \tag{12}$$

τ_w was assumed uniform from the wall to the near-wall grid point. Thus,

$$y_p^+=C_D^{1/4}\rho k_p^{1/2}\delta/\mu_{\text{lam}} \tag{13}$$

If $y_p^+\geq 11.5$, the wall shear stress (τ_w) was calculated using the formula

$$\tau_w=C_D^{1/2}\rho k_p=\rho C_D^{1/4}k_p^{1/2}(u/u^+)$$
$$=\kappa C_D^{1/4}\rho u_p k_p^{1/2}/\ell n(E\rho\delta C_D^{1/4}k_p^{1/2}/\mu_{\text{lam}}) \tag{14}$$

where

$$u^+\equiv \ell n(Ey_p^+)/\kappa \tag{15}$$

Wall shear stress was evaluated for $y_p^+<11.5$ from the formula

$$\tau_w=\mu_{\text{lam}}u_p/\delta \tag{16}$$

Due to the steep gradients of properties in turbulent flows near solid boundaries, the source terms for k and ϵ at near-wall nodes were expressed in terms of the wall shear stress.[3,9] τ_w also provides the boundary condition for the u and v equations. In the following equation for turbulence dissipation rate (ϵ) at a near-wall node (p), the length scale is presumed proportional to the distance from the wall (δ):

$$\epsilon_p=C_D^{3/4}k_p^{3/2}/\kappa\delta=k_p^{3/2}/2.43\delta \tag{17}$$

It was found, as was previously found by Netzer,[1] that (when using the sudden expansion geometry in reacting flows) the near-wall dissipation had to be increased on the step face ($\epsilon_p=k_p^{3/2}/0.4\delta$) and that the grid spacing adjacent to the fuel surface had to be fine ($y_p^+<11.5$) in order to obtain a temperature distribution in qualitative agreement with experiment. Equation (16) implies that the wall shear stress is calculated assuming a linear velocity profile when $y_p^+<11.5$. A near-wall grid point, therefore, can lie within the laminar sublayer, but the source terms for k and ϵ imply that $\mu_{\text{eff}}/\mu_{\text{lam}}$ is much greater than unity.[5,6] This precludes y_p^+ from being significantly less than 11.5.

For reacting flows, the boundary conditions for the dimensionless properties [Eqs. (7-9)] were zero at the inlet and unity "deep" in the fuel grain (fg). These properties were considered to have zero gradients on nonreacting surfaces.

The assumptions employed for reacting flows [unity turbulent Prandtl and Schmidt numbers, simple chemical reaction, constant specific heat, and stagnation enthalpy defined in Eqs. (4) and (6)] result in a general boundary condition for all "conserved" properties (ϕ_c)[8] on a surface which has mass transfer

$$\dot{m}''_{bw}=\left(\Gamma_\phi\frac{\partial\phi_c}{\partial r}\right)_{bw}\Big/(\phi_{c_{bw}}-\phi_{c_{fg}}) \tag{18}$$

where ϕ_c represents $\tilde{h}$, m_{N2}, or $\chi\equiv m_{\text{fu}}-m_{\text{ox}}/i$.

A mass transfer conductance (g) is often defined such that

$$\left(\Gamma_\phi\frac{\partial\phi_c}{\partial r}\right)_{bw}=g(\phi_{c_\infty}-\phi_{c_{bw}}) \tag{19}$$

where ϕ_{c_∞} is defined as the freestream value. For this application, ϕ_{c_∞} was taken to be the local near-wall value ϕ_{c_p}.

Substituting Eq. (19) into Eq. (18) yields

$$\dot{m}''_{bw}=g(\phi_{c_p}-\phi_{c_{bw}})/(\phi_{c_{bw}}-\phi_{c_{fg}}) \tag{20}$$

$$\equiv g\text{BP} \tag{21}$$

where BP represents the mass transfer (or "blowing") parameter. g can be approximated using[8]

$$g=(\rho u)_p St \tag{22}$$

From Reynolds analogy with unity Prandtl number,

$$St=C_f/2=\tau_w/(\rho u^2)_p \tag{23}$$

where C_f is the local friction coefficient. Thus,

$$g=\tau_w/u_p \tag{24}$$

Using the Couette flow approximation for the boundary-layer behavior with mass transfer,[8]

$$g=g^*\ell n(1+\text{BP})/\text{BP} \tag{25}$$

where

$$g^*\equiv\lim_{\text{BP}\to 0}(g) \tag{26}$$

In this application, BP was evaluated from the solution of the energy equation using

$$\text{BP}=(\tilde{h}_p-\tilde{h}_{bw})/(\tilde{h}_{bw}-\tilde{h}_{fg}) \tag{27}$$

The wall shear stress was calculated using Eq. (14) or Eq. (16) and modified with Eq. (25).

$$\tau_{bw} = \tau_w \ell n(1+\mathrm{BP})/\mathrm{BP} \tag{28}$$

where τ_w is the wall shear stress without wall mass addition.

The mass transfer conductance (g) was found using Eq. (24). The wall mass flux was then evaluated using Eq. (21).

The wall heat flux ($\dot{q}''_w$) on all solid isothermal boundaries was evaluated using the Reynolds analogy

$$-\dot{q}''_w/(\tilde{h}_p - \tilde{h}_w) = \tau_w/u_p \tag{29}$$

Since the blowing rates were small for the solid fuel ramjet (typically, BP < 2.0), k and ϵ were evaluated using Eq. (3) and the terms presented in Table 2 which incorporate the empirical constants of Table 1.

Five variables (u,v,k,ϵ, and H or $\tilde{h}$) were solved using Eq. (3) in finite-difference form. The line by line iterative procedure employed upwind differencing and under relaxation to promote convergence.[3] On each radial line, the mass flow rate was calculated using the local density. The error in mass flow (compared to the summation of "mass-in" at all upstream boundaries) was used to uniformly adjust the axial velocity over the entire line. This process ensured that overall continuity was satisfied on the line. Then, the pressure at all downstream locations was adjusted to approximately correct for the momentum imbalance created by the uniform axial velocity adjustment and a "pressure correction" equation was solved for each cell on the line. Finally, local cell velocity (axial and radial) and pressure were adjusted to satisfy cell-wise continuity. The details of this procedure are presented in Ref. 3.

Results and Discussion

The purpose of this study was to develop a primitive-variable, finite-difference computer program that could be used to determine the flow within a solid fuel ramjet combustor with emphasis on the aft mixing chamber. The effects of inlet mass flow rate and inlet dump area ratio on the flowfield were examined. As previously explained, an aft mixing region allows further combustion aft of the fuel grain. This process normally increases combustion efficiency. Lowering the inlet flow rate increases the fuel-air ratio within the fuel port; bypass air can then be injected into the aft mixing region. The latter procedure can be used to appreciably increase fuel loading.

Figure 3 shows that the fuel regression rate predictions of the u-v-p (primitive-variable) and the ψ-ω models are quite similar. Also shown are experimental data obtained with 1) axial flow through a single pipe upstream of the fuel inlet, and 2) two inlet pipes at 45 deg to the engine axis upstream of the fuel inlet. Inlet turbulence/distortion is observed to affect the axial variation of fuel regression rate. Both models predict the maximum regression rate to occur upstream of the experimental data and have similar slopes. This early peak in the regression rate results from the models predicting a shorter reattachment length than was found experimentally.[1] The primitive-variable model predicted higher regression rates downstream of flow reattachment in better agreement with experiment.

It has been found experimentally that the regression rate of plexiglas varies as the air mass flux raised to a constant power ($\dot{r}_{fu} \sim G^n$). Boaz and Netzer[10] determined this exponent to be 0.41, while Mady et al.[11] found it to be approximately 0.38. For the three cases considered in this study, the u-v-p model resulted in an exponent between 0.31 and 0.34. Thus, the primitive-variable model appears to reasonably predict the nature of the change in convective heat flux to the fuel surface with air flow rate.

Figure 4 compares the predicted centerline turbulence intensity (assuming isotropic turbulence) and experimental

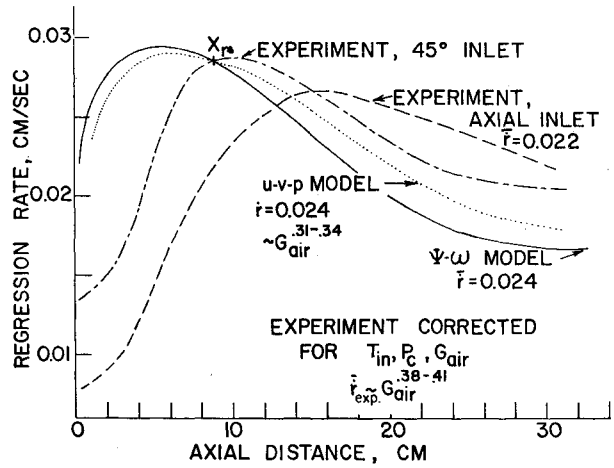

Fig. 3 Plexiglass regression rates.

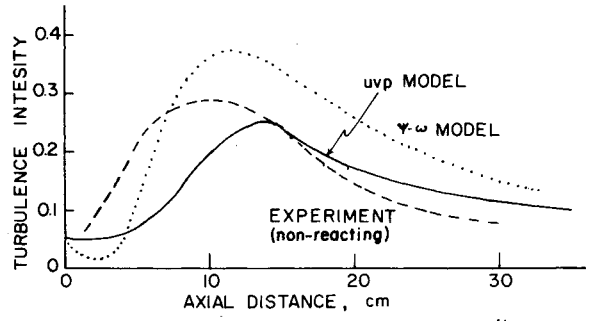

Fig. 4 Centerline turbulence intensity, $I \equiv (\frac{2}{3}k)^{1/2}/u$.

data for nonreacting flow. The primitive-variable computer model slightly underpredicted the peak turbulence intensity, while the ψ-ω model overpredicted it. Both models predicted the peak to occur downstream of the experiment and both distributions appear to approach an identical value downstream. The decrease in turbulence intensity near the inlet, which was predicted using the ψ-ω model, resulted from that model overpredicting the velocity increase as the air entered the combustor.[1] The u-v-p model overcame this difficulty. The differences in the results from the two computer models may result from the differences in the boundary conditions on turbulence kinetic energy in the combustor and/or to the effects of the addition of the aft mixing chamber on the upstream flow. It should also be noted that the experimental data used in this comparison were obtained in a nonreacting flow.

Figure 5 shows the effect of inlet velocity on the axial pressure distributions for the three primitive-variable test conditions (Table 3). The radial location of these pressure distributions is given as a fraction of the fuel port radius (R_{fp}). As expected, pressure initially increased due to jet spreading. This was followed by a slight pressure drop as the flow accelerated because of heat addition and wall friction. The final pressure rise was due to jet spreading in the aft mixing region.

Figure 6 displays radial temperature variations in the combustor near the end of the fuel grain and at about 1.5 aft mixing region diameters down the aft chamber. As previously discussed, fuel flow rate decreases less than inlet air flow rate ($\dot{r}_{fu} \sim G^n, n<1$). Therefore, as air flow rate is decreased, the overall mixture ratio becomes more fuel rich, and the developing boundary layer and the fuel layer between the diffusion flame and the wall thicken. Thus (Fig. 6), as the inlet velocity (and, therefore, the inlet air mass flux) was decreased, the maximum temperature (or "flame") in the combustor moved away from the fuel grain and the centerline temperature increased. The maximum temperature in the aft

Table 3 Solid fuel ramjet test conditions

Case	r_{in}, m	$\dot{m}_{air}$, kg/s	u_{in}, m/s	G, kg/m^2-s
1	0.00681	0.08049	1.97.0	70.6
2	0.00681	0.07274	178.0	63.8
3	0.00681	0.06442	157.6	56.5

mixing chamber was also predicted to occur farther from the wall. A significant difference between the predictions of the two computer models was that the ψ-ω model predicted a stronger dependence of the peak temperature radial location on the inlet air velocity (Fig. 8 of Ref. 1). An aft mixing region was not incorporated into the ψ-ω model. Therefore, the boundary layer continued to grow, and the point of maximum temperature continued to recede from the fuel surface with increasing axial distance from the initial reattachment point. The aft mixing region of the u-v-p model caused the boundary-layer thickness (and, therefore, the location of the peak temperature) to become approximately constant in the latter portion of the combustion chamber. This was the apparent cause of the weaker dependence predicted by the u-v-p model of peak temperature location and boundary-layer thickness on inlet air mass flux.

Figure 7 is an illustration of the predicted combustion behavior in the aft mixing region. (The radial dimension has been expanded for clarity.) Lines of maximum temperature (i.e., the flame sheet location) are presented as a function of fuel grain inlet air velocity. It should be noted that the aft recirculation zone, which is also depicted on this figure, was predicted to be fuel rich and did not vary appreciably in size with changing inlet air mass flux. As previously discussed, the fuel regression rate decreased more slowly than inlet air flow rate. Thus, as air flux was decreased, the mixture entering the aft chamber became more fuel rich and the thickness of the fuel layer at the end of the fuel grain increased slightly. With high air mass flux through the fuel port, the overall mixture ratio was fuel lean. The flame therefore propagated to the outer wall of the aft mixing chamber. This condition could be expected to produce a high combustion efficiency. It should be noted that an adequate length-to-diameter ratio is required to allow the flame to spread to the wall. This ratio is a function of the fuel port to aft mixing chamber cross-sectional area ratio. As the air flow rate was decreased, the mixture ratio became fuel rich and the flame did not reach the wall. This would result in unburned fuel entering the nozzle and a lower combustion efficiency. Figure 8 shows the predicted effect of the inlet area ratio (A_3/A_{in}) on the flame behavior in the aft mixing chamber. The recirculation zone did not change in size since the air mass fluxes were identical. The larger inlet area (A_{in}) resulted in a slightly higher fuel regression rate and therefore required a longer aft mixing region. Bypass air is sometimes used to complete the mixing/combustion aft of the fuel grain. To be effective it probably should be introduced far enough upstream for mixing/reaction with the fuel rich shear layer but not to the point where the aft recirculation region would be significantly disturbed, i.e., somewhere between the end of the recirculation zone and where the flame reaches the wall. The model predictions (Fig. 8) could be used as a first approximation for predicting this location for the bypass air dumps in the aft mixing region. To predict an optimum location, however, the primitive-variable model would have to be expanded to three dimensions.

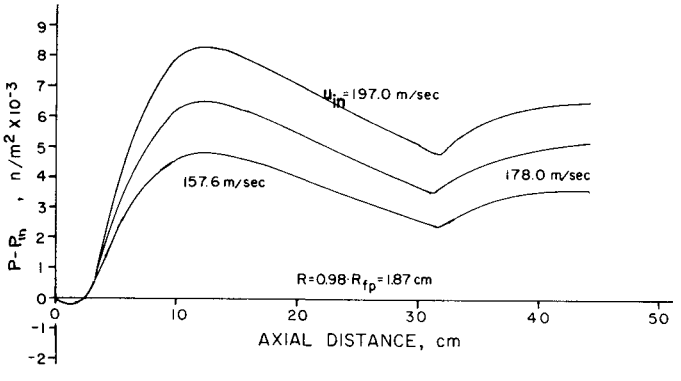

Fig. 5 Predicted axial pressure distributions.

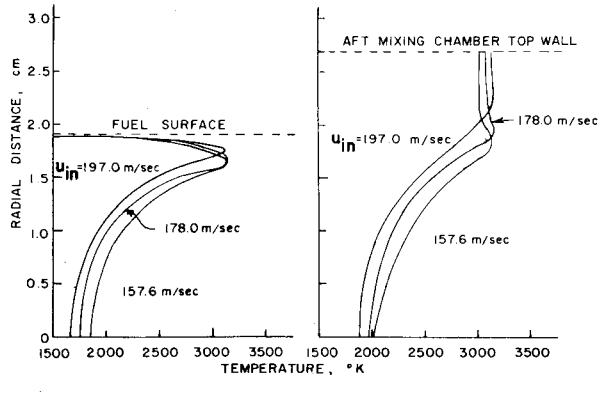

Fig. 6 Predicted fuel grain and aft mixing chamber radial temperature profiles.

Computer-Related Problems

As has been discussed previously, in order to obtain results that were in agreement with experiment, the grid spacing near the fuel surface was required to be fine and the length scale of turbulence was decreased on the combustor step face. Because convergence was sensitive to the length-to-width ratio of individual control volumes, the small radial grid spacing near the fuel surface forced similar fine spacing in the axial direction downstream in the aft mixing region. A length-to-width ratio of less than ten to one was required. These criteria forced the use of a large number of cells, which in turn required a large amount of CPU time. A typical grid size was 40 × 33 and required 75-80 min of CPU time on an IBM 360-67 computer to converge.

The primitive-variable model experienced some convergence difficulty in the aft recirculation region. This

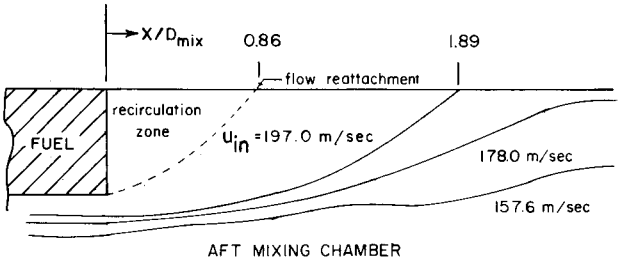

Fig. 7 Effect of air flow rate on predicted flame location in aft mixing region.

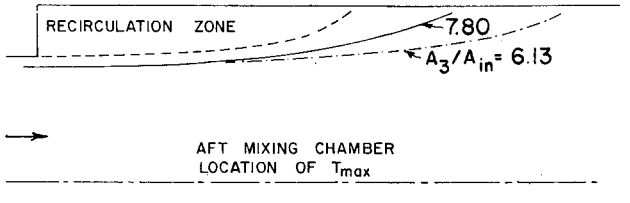

Fig. 8 Effect of fuel grain inlet, geometry on flame zone in the aft mixing region.

problem seemed to be associated with the continually changing velocity profile just prior to the aft expansion (the "inlet" conditions for the aft mixing chamber). This effect was suppressed by sweeping through the entire flowfield several times with only a few traverses on each line and then increasing the number of traverses on the radial grid lines in the aft mixing region once the flowfield within the fuel grain had essentially converged.

Conclusions

In general, the predicted flowfields for the two computer models were quite similar within the fuel grain. However, the presence of the aft mixing region coupled with the few boundary condition differences previously mentioned had some effect on the flowfield predictions. The most noticeable of these was the decrease in dependence of the boundary-layer thickness and the maximum temperature radial location on axial inlet velocity. As anticipated, the primitive-variable model readily permitted the prediction of the flowfield within the aft mixing region. Many additional empirical data are needed to completely assess the validity of the primitive-variable model for predicting the flow in a solid-fuel ramjet.

Acknowledgment

This work was sponsored by the Naval Weapons Center, China Lake, California.

References

[1] Netzer, D.W., "Modeling Solid-Fuel Ramjet Combustion," *Journal of Spacecraft and Rockets*, Vol. 14, Dec. 1977, pp. 762-766.

[2] Netzer, D.W., "Model Applications to Solid-Fuel Ramjet Combustion," *Journal of Spacecraft and Rockets*, Vol. 15, Sept.-Oct. 1978, pp. 263-264.

[3] Pun, W.M. and Spalding, D.B., "A General Computer Program for Two-Dimensional Elliptic Flows," Imperial College of Science and Technology, Rept. No. HTS/76/2, Aug. 1977.

[4] Mongia, H.C. and Reynolds, R.S., "Combustor Design Criteria Validation Volume III," AIRESEARCH Manufacturing Co. of Arizona, Report. No., USARTL-TR-78-55 c, Feb. 1979.

[5] Launder, B.W. and Spalding, D.B., "The Numerical Computation of Turbulent Flows," *Computer Methods in Applied Mechanics and Engineering*, Aug. 1973, pp. 269-289.

[6] Jones, W.P. and Launder, B.E., "The Predictions of Laminarization with a Two-Equation Model of Turbulence," *International Journal of Heat and Mass Transfer*, Vol. 15, 1972, pp. 68-87.

[7] Launder, B.E. and Spaulding, D.B., Lectures in Mathematical Models of Turbulence, 2nd Ed., Academic Press, 1976, pp. 95-102.

[8] Kays, W.M., Convective Heat and Mass Transfer, McGraw-Hill, 1966, pp. 300-313 & 326-328.

[9] Gosman, A.D. et al., Heat and Mass Transfer in Recirculating Flows, Academic Press, 1969, pp. 69-74 & 119-123.

[10] Boaz, L.D. and Netzer, D.W., "An Investigation of the Internal Ballistics of Solid Fuel Ramjets," Naval Postgraduate School, Monterey, Calif., Report No. NPS-67Nt-73031A, March 1973.

[11] Mady, C.J., Hickey, P.J., and Netzer, D.W., "Combustion Behavior of Solid Fuel Ramjets," *Journal of Spacecraft and Rockets*, Vol. 15, May-June 1978, pp. 131-132.